Chinese Chemical Letters 36 (2025) 110241

Contents lists available at ScienceDirect

Chinese Chemical Letters

journal homepage: www.elsevier.com/locate/cclet

Tetrahedral framework nucleic acids enhance osteogenic differentiation and prevent apoptosis for dental follicle stem cell therapy in diabetic bone repair

Ruijianghan Shi[a,b], Yujie Zhu[a,b], Weitong Lu[a,b], Yuhan Shao[a,b], Yang Chen[c], Mi Zhou[a,b], Yunfeng Lin[a,b], Sirong Shi[a,b,*]

[a] State Key Laboratory of Oral Diseases & National Center for Stomatology & National Clinical Research Center for Oral Diseases, West China Hospital of Stomatology, Sichuan University, Chengdu 610041, China
[b] Sichuan Provincial Engineering Research Center of Oral Biomaterials, Chengdu 610041, China
[c] Department of Pediatric Surgery, Department of Liver Surgery & Liver Transplantation Center, West China Hospital of Sichuan University, Chengdu 610041, China

ARTICLE INFO

Article history:
Received 21 May 2024
Revised 9 July 2024
Accepted 10 July 2024
Available online 14 July 2024

Keywords:
Tetrahedral framework nucleic acids
DNA nanomaterials
Diabetes mellitus
Dental follicle stem cells
ROS/MAPKs/NF-κB pathway

ABSTRACT

Hyperglycemia resulting from diabetes mellitus (DM) exacerbates osteoporosis and fractures, damaging bone regeneration due to impaired healing capacity. Stem cell therapy offers the potential for bone repair, accelerating the healing of bone defects by introducing stem cells with osteogenic differentiation ability. Dental follicle stem cells (DFSCs) are a newly emerging type of dental stem cells that not only have the potential for multipotent differentiation but also hold easy accessibility and can stand long-term storage. However, DM-associated oxidative stress and inflammation elevate the risk of DFSCs dysfunction and apoptosis, diminishing stem cell therapy efficacy. Recent nanomaterial advances, particularly in DNA nanostructures like tetrahedral framework nucleic acids (tFNAs), have been promising candidates for modulating cellular behaviors. Accumulating experiments have shown that tFNAs' cell proliferation and migration-promoting ability and induce osteogenic differentiation of stem cells. Meanwhile, tFNAs can scavenge reactive oxygen species (ROS) and downregulate the secretion of inflammatory factors by inhibiting various inflammation-related signaling pathways. Here, we applied tFNAs to modify DFSCs and observed enhanced osteogenic differentiation alongside ROS scavenging and anti-inflammatory effects mediated by suppressing the ROS/mitogen-activated protein kinases (MAPKs)/nuclear factor kappa-B (NF-κB) signaling pathway. This intervention reduced stem cell apoptosis, bolstering stem cell therapy efficacy in DM. Our study establishes a simple yet potent tFNAs-DFSCs system, offering potential as a bone repair agent for future DM treatment.

Diabetes mellitus (DM), a universal chronic disease affecting a great global populace, is rapidly increasing owing to socioeconomic advancements, shifts in lifestyle, and demographic aging [1]. Hyperglycemia, prevalent among DM patients, is a principal pathophysiological cause of DM and its associated complications [2]. DM affects bone metabolism, precipitating osteoporosis [3], thereby heightening the susceptibility to fractures, resulting in prolonged immobilization and consequent morbidity and mortality [4]. Moreover, the inflammatory microenvironment, dysregulated metabolic turnover of osteoblasts and osteoclasts, reactive oxygen species (ROS), and heightened vulnerability to infections induced by DM can damage bone regeneration [5]. Consequently, addressing bone fragility and regeneration deficiencies in individuals with DM remains a great clinical challenge and a topic of intense investigation [6].

Stem cell transplantation has emerged as a promising modality for bone repair, drawing significant attention due to its biological efficacy [7]. Among these stem cells, dental follicle stem cells (DFSCs), a novel type of dental mesenchymal stem cells (MSCs), which is a promising candidate for regenerative medicine and tissue engineering, particularly in the orofacial domain [8,9]. DFSCs exhibit a repertoire of pluripotent genes and can be differentiated into three distinct DF cell lines [10], revealing their multipotent differentiation potential [11]. Moreover, DFSCs offer the advantage of easy accessibility, as they can be conveniently harvested from discarded

* Corresponding author.
E-mail address: sirongshi@scu.edu.cn (S. Shi).

https://doi.org/10.1016/j.cclet.2024.110241
1001-8417/

teeth, and the feasibility of cryopreserving dental follicle tissue for future DFSC utilization [12]. Consequently, DFSCs are emerging as a promising resource for stem cell-based regenerative therapies.

However, stem cell therapy encounters numerous challenges in DM patients, including chronic inflammation, senescence, hypoxia, oxidative stress, mitochondrial dysfunction, and programmed cell death, which can impair stem cell functionality and diminish therapeutic efficacy [13-15]. Extensive research has demonstrated that the hyperglycemic microenvironment in DM induces excessive oxidative stress, thereby impairing osteogenic differentiation [16] and activating the ROS/mitogen-activated protein kinases (MAPKs)/nuclear factor kappa-B (NF-κB) signaling pathway [3], eventually resulting in cell apoptosis in both intrinsic and extrinsic pathways [17,18]. Hence, there is a pressing need for strategies targeting the ROS/MAPKs/NF-κB pathway to facilitate DFSCs therapy in DM patients.

In recent years, with advancements in nanomaterials, DNA nanostructures have garnered attention for their diagnostic [19], therapeutic, and drug-delivery potentials [20-27]. Among these, tetrahedral framework nucleic acids (tFNAs), constructed from four single-stranded DNAs (ssDNA), exhibit three-dimensional structures endowed with design flexibility, stability in complex environments, and specificity in modification [28]. Accumulating evidence suggests that in DM conditions, tFNAs exert favorable effects on cellular behaviors including proliferation, migration [29,30], osteogenic differentiation induction [31,32], anti-inflammatory properties [33-35], and resistance to oxidative stress [5,28]. However, to date, no investigations have examined the impact of tFNAs on stem cell dysfunction in DM conditions.

In this study, we simulate an inflammatory and oxidative microenvironment by creating a high glucose environment *in vitro* and subsequently treating DFSCs with tFNAs to assess their effects. Initially, we evaluate whether tFNAs confer protective effects on the osteogenic differentiation of DFSCs under high glucose conditions. Subsequently, we delve into oxidant-associated markers, apoptosis-related factors, and signaling pathways *in vitro* to elucidate the underlying mechanisms. Our findings demonstrate that in high glucose conditions, tFNAs enhance the osteogenic differentiation of DFSCs and mitigate stem cell dysfunction by suppressing the ROS/MAPKs/NF-κB pathway, offering a novel strategy to augment the therapeutic efficacy of DFSCs in DM bone regeneration. All experimental materials and methods are detailed in Section 1 (Supporting information).

According to Fig. 1a, equimolar amounts of each single-stranded DNA facilitated self-assembly into a triangular structure, subsequently pairing with other ssDNA to construct a tetrahedral configuration following a particular base complementation pairing rule. The observed result in Fig. 1b by high performance capillary electrophoresis (HPCE) indicated a single strand length of approximately 40 bp and a tFNA molecule size of about 160 bp, consistent with theoretical values reported [36]. The successful tFNAs synthesis was confirmed through polyacrylamide gel electrophoresis (PAGE) in Fig. 1c, which displays the relative molecular weight relationship between ssDNA single strand and tFNAs in sequence. Subsequent exploration utilizing dynamic light scattering (DLS) revealed an average zeta potential of approximately −9.17 mV and an average size of approximately 10.7 nm for tFNA molecules (Figs. 1d and e). Further validation of tFNAs synthesis employed transmission electron microscopy (TEM) and atomic force microscope (AFM) to examine morphology and average size, as depicted in Figs. 1f and g, manifesting shapes akin to triangles and an average particle size of approximately 10 nm for each tFNAs. Collectively, these findings affirm the successful self-assembly of tFNAs.

Successful extraction of DFSCs was evidenced by the detection of DFSCs-specific surface marker CD90 (Fig. 1h) [37]. Additionally, cell immunofluorescence staining depicted a high expression of

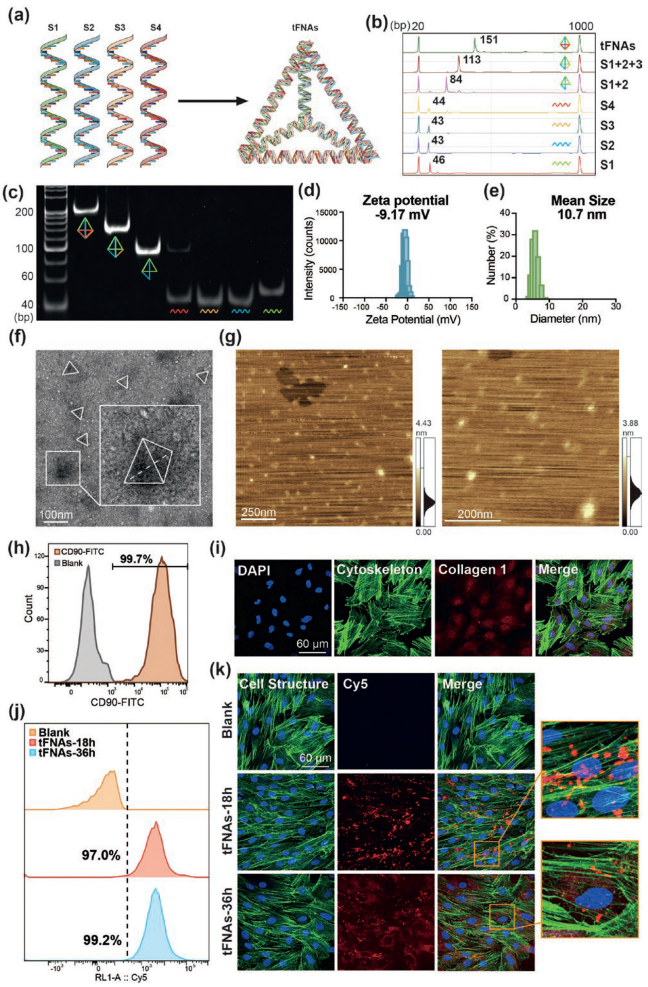

Fig. 1. Synthesis, characterization, and cellular uptake of tFNAs, and authentication of DFSCs. (a) The synthesis of tFNAs. (b, c) HPCE (b) and PAGE (c) of tFNAs. (d) Zeta potential distribution. (e) Size distribution. (f) TEM image. Scale bar: 100 μm. (g) AFM image. Scale bars: 250 and 200 μm. (h) Flow cytometry of CD90. (i) Immunofluorescence detection of collagen I. Scale bar: 60 μm. (j) Flow cytometry of cellular uptake of Cy5-tFNAs. (k) Fluorescent imaging of cellular uptake of Cy5-tFNAs. Scale bar: 60 μm. DAPI, 4′,6-diamino-2-phenylindole.

collagen I, indicative of the osteogenic differentiation potential of DFSCs (Fig. 1i), consistent with prior investigations [38].

The mechanism underlying the cellular endocytosis of tFNAs has been extensively studied. Beyond the widely recognized caveolin-mediated cell endocytosis hypothesis [39], studies have suggested microtubule-dependent tFNAs transportation [40] and potential associations with proteins such as CAV1 and SNX5 [41]. To assess the cellular internalization of tFNAs, Cy5-modified tFNAs were co-cultured with DFSCs, and tFNAs' endocytic behavior was observed at different time points (18 and 36 h). Flow cytometry results (Fig. 1j) indicated that after 18 and 36 h of co-culture, 97.0% and 99.2% of DFSCs exhibited high fluorescence intensity, signifying widespread internalization of Cy5-tFNAs by cells within 18 h of co-culture. The internalized Cy5-tFNAs remained intact inside the cells for at least 48 h, demonstrating resistance to nuclease attack. While flow cytometry revealed the endocytosis efficiency of tFNAs, immunofluorescence staining results provided insight into the tFNAs transportation process. As depicted in Fig. 1k, Cy5-tFNAs initially appeared as red fluorescence within larger vesicles, which overlapped with the cytoskeleton after 18 h of incubation. Subsequently, they partly diffused into smaller particles in the cytoplasm around the nucleus after 36 h of incubation, consistent with the

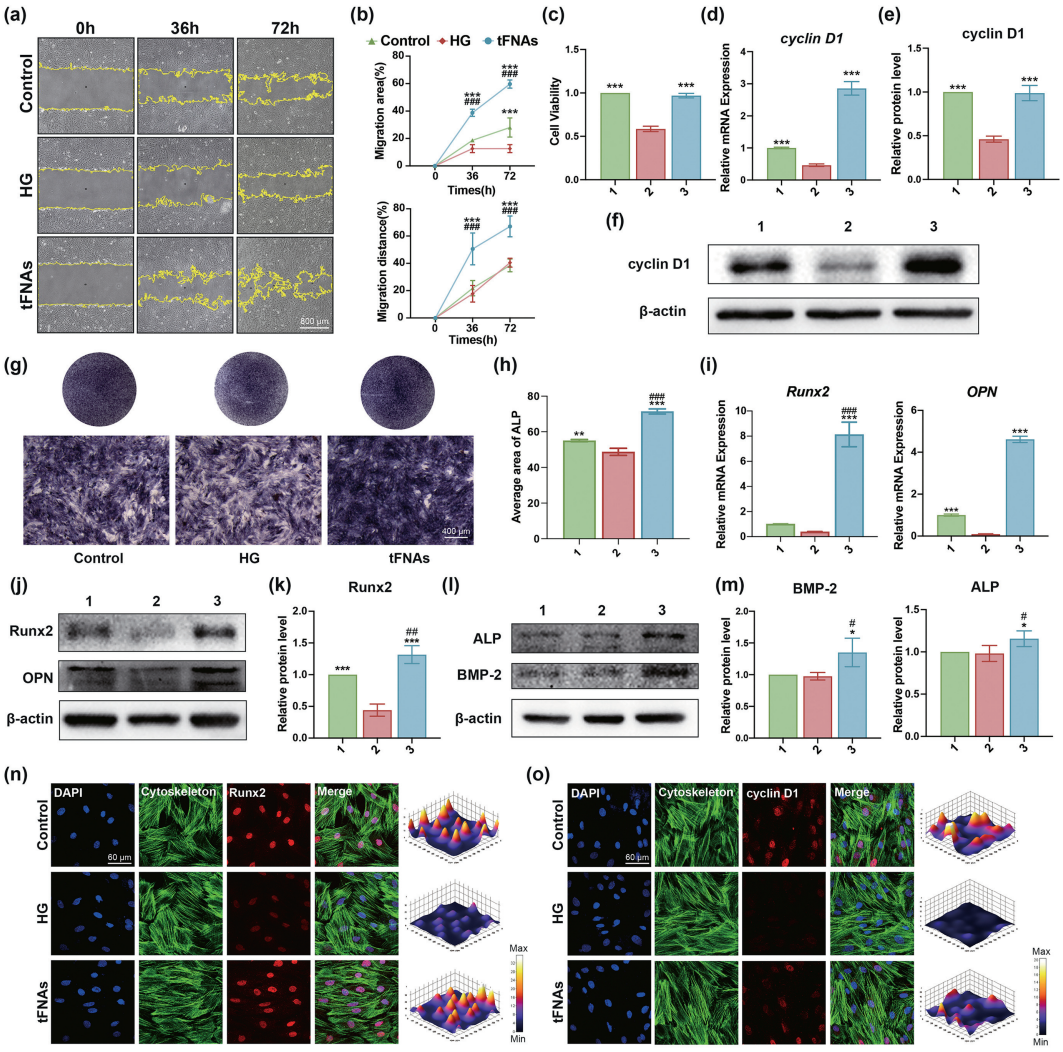

Fig. 2. tFNAs enhance cell migration, proliferation, and osteogenic differentiation of DFSCs under high glucose conditions. (a, b) Wound healing assay with statistical analysis. Scale bar: 800 μm. (c) Cell viability assay with statistical analysis. (d, i) The relative mRNA expression intensity of *cyclin D1, Runx2,* and *OPN*. (e, f, j–m) Western blot with statistical analysis detecting the protein expression levels of cyclin D1, Runx2, OPN, ALP and BMP-2 protein expression levels. (g, h) Photographs and micrographs with statistical analysis of ALP staining. Scale bar: 400 μm. (n, o) Immunofluorescence detection of Runx2 and cyclin D1. Scale bar: 60 μm. Group settings: 1-control, 2-HG, 3-HG + tFNAs. Data are presented as mean ± standard deviation (SD) ($n = 3$). $^{*}P < 0.05$, $^{**}P < 0.01$, $^{***}P < 0.001$ *vs.* HG; $^{\#}P < 0.05$, $^{\#\#}P < 0.01$, $^{\#\#\#}P < 0.001$ *vs.* control.

theory of microtubule-dependent transportation of tFNAs. Remarkably, tFNAs, as nucleic acid materials with a negative charge, were effectively internalized by DFSCs without requiring additional carriers. This observation laid the groundwork for subsequent experiments.

MSCs are known for their homing ability, enabling migration into injured sites. MSCs can also differentiate into local components, along with the secretion of chemokines, cytokines, and growth factors crucial for tissue regeneration [42,43]. This intrinsic ability contributes to stem cell therapy in bone repair models. Nevertheless, challenges arise when MSCs encounter high glucose (HG) conditions, significantly impairing their migration and proliferation abilities [44]. Following tFNAs internalization, mounting evidence suggests their crucial role as regulators in cell behaviors, including cell proliferation and migration. Scratch experiments were conducted to observe cell migration behavior. DFSCs were separated into three groups, and the HG + tFNAs groups received tFNAs at a concentration of 250 nmol/L, while other groups received 250 nmol/L phosphate buffered saline (PBS). Results depicted in Fig. 2a revealed that HG hindered the migration rates of DFSCs yet was restored following treatment with tFNAs. Statistical analysis involved indirect measurement of the remaining space and distance (Fig. 2b) of the wound, with subsequent calculation of ratios. After 36 h, migration area, and migration distance percentages were 18.68% and 21.81% in the control group, 12.6% and 17.73% in the HG group, and 38.76% and 50.59% in the tFNAs group, respectively. After 72 h, statistics for the control group reached 28.01% and 38.51%. The tFNAs group achieved 59.71% and 67.06%, while in the HG group, these percentages only increased to 23.97% and 40.49%.

Cell proliferation was assessed using the cell counting kit-8. As depicted in Fig. 2c, a decline in cell proliferation was observed when DFSCs were exposed to HG conditions (down to 0.58-fold). Conversely, HG-stimulated cells treated subsequently with tFNAs (250 nmol/L) demonstrated enhanced cell viability (up to 1.65-fold). Cyclin D1 is a protein regulating cell proliferation behavior, which binds and activates the cyclin-dependent kinase 4 (CDK4) to initiate transcription of genes related to the active cell cycle, thereby driving the cell cycle from the G1 phase to the S phase [45]. Multiple assays were employed to assess cyclin D1 expression at both the genetic and protein levels to further delve into the proliferative potential promoted by tFNAs. At the gene level,

reverse transcription-polymerase chain reaction (RT-PCR) analysis demonstrated a significant increase in *cyclin D1* mRNA levels in the tFNAs group (up to 6.2-fold compared to the HG group) despite the inhibitory effect of HG conditions (down to 0.46-fold compared to the control group) (Fig. 2d). Protein analysis (Figs. 2e and f) *via* Western blot revealed a significant decrease in cyclin D1 expression after incubation in HG conditions (down to 0.46-fold). However, exposure to 250 nmol/L tFNAs for 24 h significantly increased by 2.14-fold compared to the HG group. Consistently, immunofluorescence images corroborated the Western blot results, confirming higher cyclin D1 expression at the protein level (Fig. 2o). These findings revealed the robust potential of tFNAs in promoting cell migration and proliferation, thereby facilitating DFSCs to exert their homing function in bone defects, consequently enhancing the efficacy of cell therapy for achieving notable therapeutic outcomes.

Furthermore, tFNAs influence various signaling pathways to enhance MSCs' osteogenic differentiation. Nevertheless, reports indicate a notable reduction in the osteogenic differentiation capacity of MSCs under HG conditions [46]. To explore whether tFNAs can protect the differentiation of DFSCs during HG, a comprehensive array of osteogenic markers assays was employed. Regarding osteogenic differentiation ability, alkaline phosphatase (ALP) staining was initially employed to qualitatively assess the osteogenic differentiation states of DFSCs. In all groups cultured in an osteogenic induction medium, blue-purple precipitates were observed, indicating active ALP presence. The HG + tFNAs group exhibited the darkest coloration, followed by the control group, while the HG group appeared the lightest, suggesting enhanced ALP activity in the HG + tFNAs group (Figs. 2g and h).

The macroscopic results of ALP staining are visual evidence showcasing the bone-promoting capability of tFNAs under HG conditions. Subsequently, we aim to delve into the micro-level analysis of genes and proteins to elucidate the regulatory influence of tFNAs on bone-promoting proteins and genes. To elucidate the positive effect of tFNAs on the osteogenic differentiation of DFSCs under HG conditions over short and long terms, the expression of osteogenic markers Runt-related transcription factor 2 (Runx2), ALP, osteopontin (OPN), and bone morphogenetic protein-2 (BMP-2) was examined. As a hallmark of early osteogenic differentiation, the pivotal role of Runx2 in guiding stem cell osteogenic differentiation has garnered widespread recognition [47]. Initially, the influence of tFNAs on DFSCs in the early stages was assessed by evaluating the gene and protein expression of Runx2 and OPN after treating DFSCs under HG conditions with tFNAs (250 nmol/L) for 1 day. RT-qPCR analysis indicated HG conditions inhibited the expression of osteogenesis-related markers, decreasing Runx2 and OPN expression compared to the control group. However, tFNAs significantly mitigated this inhibitory effect, increasing these gene expressions compared to the HG group (Fig. 2i). Consistent with RT-qPCR results, Western blot and immunofluorescence analysis of Runx2 and OPN also demonstrated tFNAs' mitigation of the inhibitory impact of HG (Figs. 2j, k and n). Furthermore, long-term changes in osteogenic-associated genes were assessed by evaluating the expression of osteogenic-specific proteins ALP and BMP-2 *via* Western blot after DFSCs were treated with 250 nmol/L tFNAs for 3 days, while co-culturing with an osteogenic induction medium. The protein contents in the HG + tFNAs group exceeded the HG group, indicating increased ALP and BMP-2 expression compared to the HG group (Figs. 2l and m). These findings underscore the protective role of tFNAs in enhancing the osteogenic differentiation ability of DFSCs under high glucose conditions.

It has become widely acknowledged that high glucose environments can provoke excessive intracellular oxidative stress, marked by the overaccumulation of ROS [48]. This excessive ROS accumulation precipitates a cascade of cellular functional impairments and upregulates inflammation-related signaling pathways, inducing cells to secrete inflammatory cytokines, thus fostering an inflammatory microenvironment. However, as a novel nucleic acid material, in numerous studies, tFNAs have exhibited commendable ROS-scavenging capabilities [49-51]. They can modulate the release and expression of inflammatory cytokines through negative feedback on various inflammation-related signaling pathways. Consequently, they can potentially improve the local environment of stem cells and regulate cellular function. Based on previous research [3], the expression peaks of factors related to oxidative stress and inflammatory response pathways in cells exposed to a high-sugar environment occur within 24–48 h. During this period, these pathways are activated, and the risk of cellular dysfunction and apoptosis is at its highest. Therefore, in this section, to verify the immediate effect of tFNAs on local stem cell transplantation sites, DFSCs were separated into four groups, including the control group, the HG group, and HG + tFNAs groups consisting of tFNAs incubated for 24 and 48 h (tFNAs-24 h, tFNAs-48 h). To investigate the tFNAs' effect on excessive oxidative and inflammatory impact by HG, the production of ROS and antioxidant enzymes, and inflammatory cytokines were examined.

As depicted in Fig. 3a, ROS production in the HG group was notably upregulated, reflecting stimulation in the hyperglycemic environment. Conversely, subsequent incubation with tFNAs alleviated ROS production in DFSCs, reducing fluorescence intensity after 24 and 48 h incubation. Flow cytometry results (Fig. 3b) echoed this trend. DFSCs under HG condition exhibited higher ROS production at about 78.3%, rising from 33.3% in the normal cultured group (control); however, after tFNAs incubations, the ROS level downgraded to 35.2% and 64.2% in 24 and 48 h, showing great ROS-scavenging capabilities. Superoxide dismutase (SOD) facilitates the dismutation of O^{2-} into H_2O_2 and O_2 [52]. Subsequently, catalase (CAT) catalyzes the decomposition of H_2O_2 into oxygen and water, thereby effectively neutralizing ROS [53]. Thus, regarding antioxidant ability, the secretion of SOD and CAT was evaluated at both the gene and protein levels. Enzyme activity of SOD decreased by 0.53-fold in DFSCs treated with HG (Fig. 3c). Following tFNAs treatment, the production of SOD increased by 1.87-fold after 24 h treatment and by 1.89-fold after 48 h treatment, compared to the HG group. RT-PCR examined similar trends in gene expression (Fig. 3d).

Oxidative stress-induced damage activates the inflammatory response in cells. To examine the inhibiting effects of excessive oxidative stress by HG and the protective efforts of tFNAs, the gene and protein expression of inflammatory factors, tumor necrosis factor-α (TNF-α) and interleukin 1β (IL-1β) were evaluated. RT-PCR analysis revealed HG significantly stimulated expressions of *TNF-α* and *IL-1β*, and subsequent tFNAs treatment inhibited the gene expressions of these mediators after 24 and 48 h (Fig. 3e). Furthermore, protein expressions of TNF-α and IL-1β were examined and semi-quantified by Western blot and immunofluorescence, revealing downregulation of inflammatory mediator release following tFNAs treatment. Protein analysis *via* Western blot (Figs. 3f and g) accord with the gene expression findings. Following HG induction, the average level of TNF-α expression increased by 1.31-fold compared to the control group. However, subsequent treatment with tFNAs for 24 and 48 h led to a notable reduction in TNF-α expression by an average of 0.71- and 0.70-fold, respectively, compared to the HG group. These results underscore the inhibitory capacity of tFNAs against inflammatory mediators. Consistent with Western blot findings, immunofluorescence (Figs. 3h and i) revealed increased levels of TNF-α and IL-1β expression following pretreatment with HG, indicative of heightened inflammatory mediator release. Subsequent treatment with tFNAs effectively downregulated the release of these inflammatory mediators.

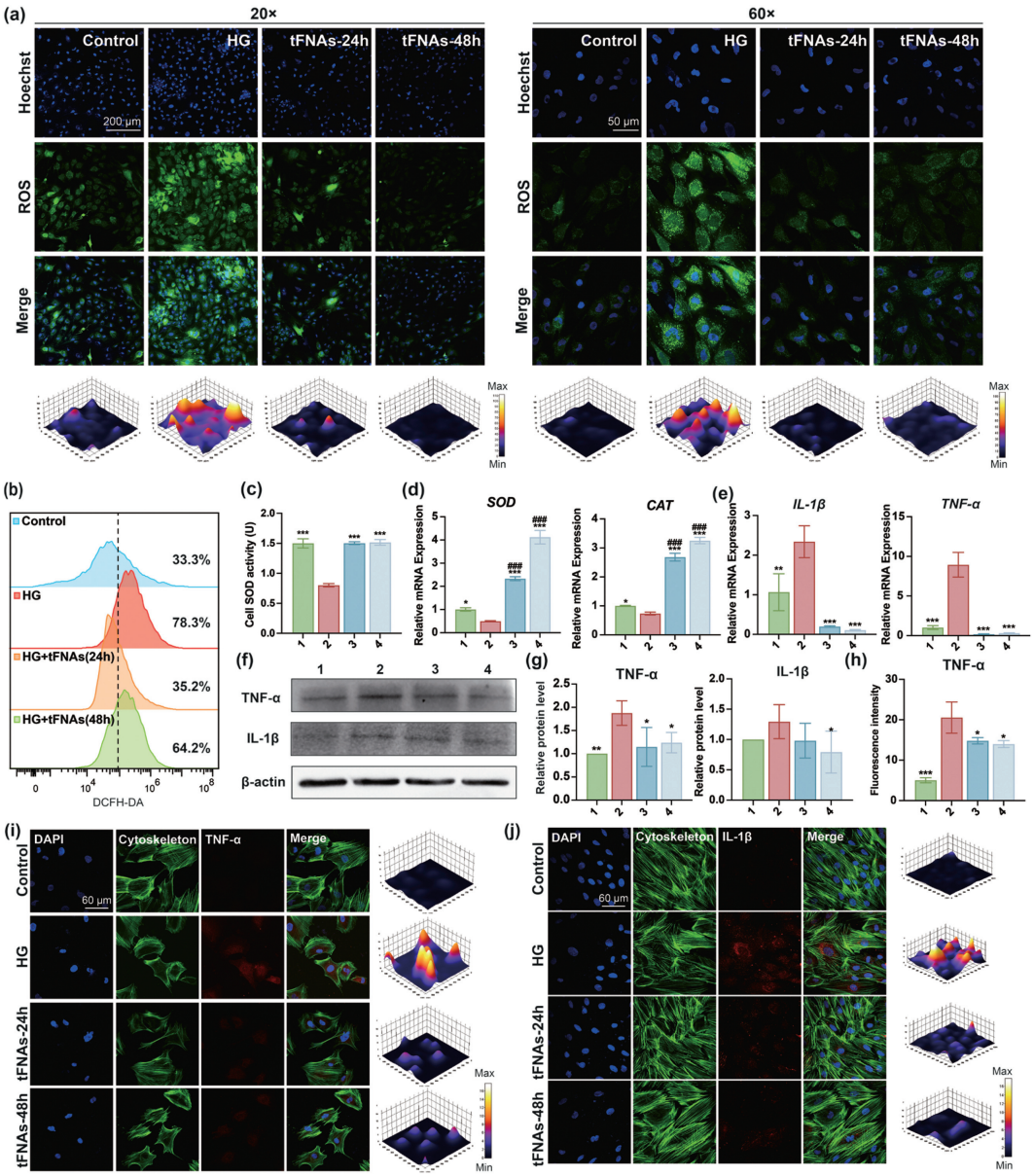

Fig. 3. Effect of tFNAs on preventing oxidative stress and control inflammation under high glucose conditions. (a) Fluorescent images of the intracellular ROS intensity. Scale bars: 200 μm (20×) and 50 μm (60×). (b) Flow cytometric results for intracellular ROS fluorescence detection. (c) The activity of antioxidant enzymes (SOD) in DFSCs with statistical analysis. (d, e) The relative mRNA expression intensity of *SOD, CAT, IL-1β* and *TNF-α*. (f, g) Western blot with statistical analysis detects IL-1β and TNF-α protein expression levels. (h–j) Immunofluorescence detection with statistical analysis of IL-1β and TNF-α. Scale bar: 60 μm. Group settings: 1-control, 2-HG, 3-HG + tFNAs (24 h), 4-HG + tFNAs (48 h). Data are presented as mean ± SD ($n = 3$). $^{*}P < 0.05$, $^{**}P < 0.01$, $^{***}P < 0.001$ *vs.* HG; $^{\#}P < 0.05$, $^{\#\#}P < 0.01$, $^{\#\#\#}P < 0.001$ *vs.* control.

Both oxidative stress and inflammation contribute to cellular dysfunction [54-56] and even apoptosis [57-59]. Thus, timely inhibition and regulation of these injurious states are imperative for cell therapy under HG conditions, as they directly impact stem cells' short-term viability and long-term cellular behavior. Our experimental findings strongly support the ROS scavenging capability of tFNAs and their anti-inflammatory effects. Additionally, tFNAs have been demonstrated to prevent and treat oxidative stress damage by activating the protein kinase B (Akt)/erythroid 2-related factor 2 (Nrf2) pathway [50], highlighting their comprehensive antioxidant performance. Our research demonstrates that tFNAs effectively counteract the "oxidative stress-inflammatory" synergistic response activated under HG conditions through multiple targets, underscoring their potent antioxidant and anti-inflammatory properties and their considerable potential for cell therapy in DM patients.

Following excessive oxidative stress and local inflammatory microenvironment, the cell apoptotic pathway is activated, comprising intrinsic and external pathways. In DM patients, where potential internal and external apoptosis pathways are activated, stem cells face a significant risk of widespread apoptosis. Based on previous research, tFNAs have demonstrated a protective effect against cell apoptosis induced by accumulated oxidative damage and inflammatory injury [60]. To evaluate the immediate therapeutic effect of tFNAs on local stem cell transplantation sites, DFSCs were separated into four groups, including the control group, the HG group, and HG + tFNAs groups consisting of tFNAs incubated for 24 and 48 h (tFNAs-24 h, tFNAs-48 h).

An annexin V assay was employed to ascertain the veracity of the protective effect on DFSC viability following tFNAs treatment. Results revealed that treatment with tFNAs resulted in apoptosis in only a minority of cells (5.68% for 24 h, 9.65% for 48 h), com-

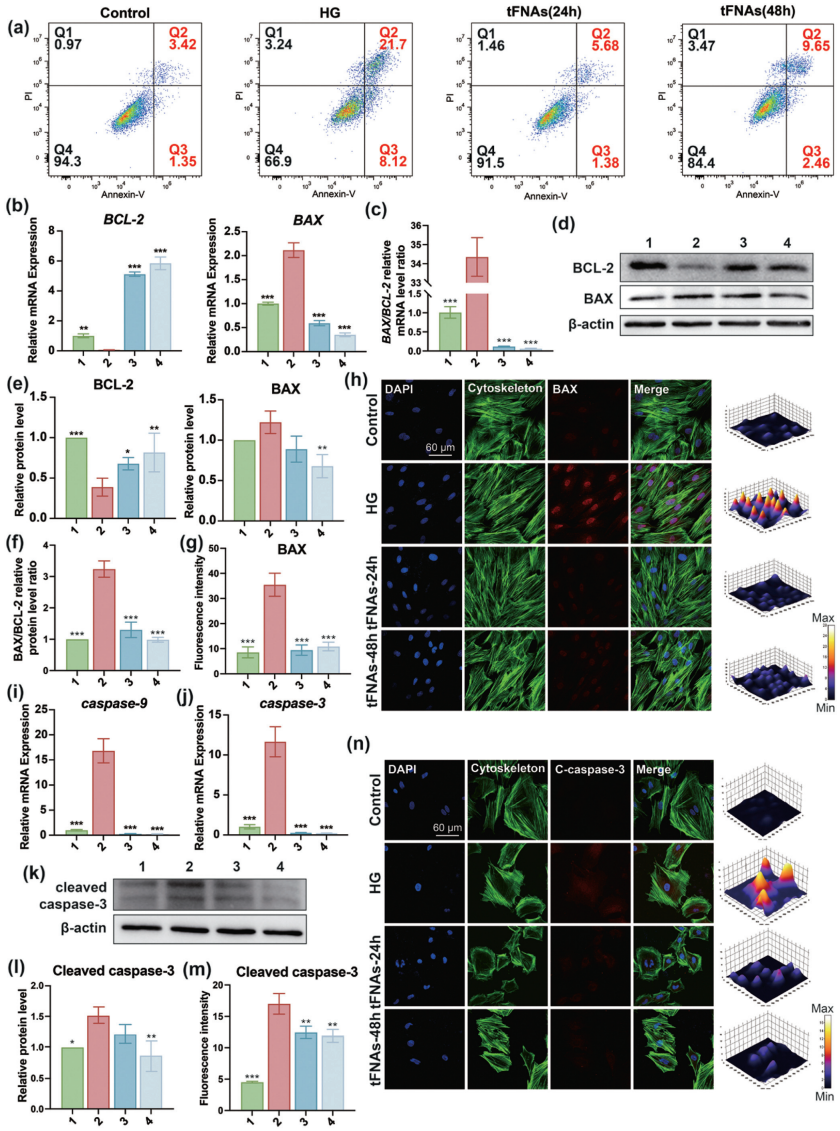

Fig. 4. tFNAs downgrade cell apoptosis under high glucose conditions. (a) Flow cytometry detecting cell apoptosis and the distribution of early and late apoptotic and viable cells. (b, i, j) The relative mRNA expression intensity of apoptosis-related genes. (d, e, k, l) Western blot with statistical analysis detects apoptosis-related protein expression levels. (g, h, m, n) Immunofluorescence detection with statistical analysis of apoptosis-related protein. Scale bar: 60 μm. (c, f) Graphs of statistical analysis of the relative mRNA and protein level of BAX/BCL-2. Group settings: 1-control, 2-HG, 3-HG + tFNAs (24 h), 4-HG + tFNAs (48 h). Data are presented as mean ± SD ($n = 3$). $^{*}P < 0.05$, $^{**}P < 0.01$, $^{***}P < 0.001$ *vs.* HG.

pared to the HG group, where a higher percentage of cells (21.7%) underwent apoptosis (Fig. 4a).

Stress including oxidative stress and inflammation impacting mitochondria, triggers the intrinsic apoptosis pathway [61,62]. The part of the BCL-2 family takes in mitochondrial apoptotic regulation is commonly depicted as an equilibrium between its anti-apoptotic factor (BCL-2) and pro-apoptotic factor (BAX), which are in constant competitive flux to influence the activation of pore-forming executioners [63,64]. Activation of the executioners leads to forming pores in the outer mitochondrial membrane, culminating in mitochondrial outer membrane permeability and subsequent apoptosis [65]. The balance between these subfamily members within cells can be modulated by various signaling pathways, effectively conveying information about cellular stress, including oxidative stress [66,67] and inflammatory environments [68,69]. BAX and BCL-2 gene expression levels were examined *via* RT-PCR (Fig. 4b). Compared to the control group, the gene levels of BAX increased, which was concomitant with a decrease in the gene levels of an apoptosis-resistant factor (*BCL-2*). Conversely, following incubation with tFNAs for 24 and 48 h, a significant increase in *BCL-2* gene expression was observed, by an average of 82.9- and 94.6-fold, respectively, and the expression of *Bax* decreased after 24 and 48 h incubation by an average of 0.57- and 0.24-fold. Additionally, gray value analysis of Western blot bands revealed that BAX in the tFNAs group after 24 and 48 h incubation decreased by 0.62- and 0.48-fold, respectively; BCL-2 expression in the tFNAs group after 24 and 48 h incubation increased by 1.54- and 1.56-fold, respectively (Figs. 4d and e). In the immunofluorescence experiments, the red fluorescence intensity corresponding to the expression of BAX was strongest in the HG group, while weak in both tFNAs and control groups (Fig. 4h). In our investigation, this mitochondrial-mediated apoptotic pathway was markedly suppressed in the presence of tFNAs. As depicted in Figs. 4c and f, both at the genetic and protein expressions, the ratio of BAX to BCL-2 substantially increased under HG conditions, signifying that HG-induced oxidative stress and ensuing inflammation significantly heightened cell

apoptosis. However, the experimental group treated with tFNAs exhibited a comparable or even reduced ratio compared to the control group.

Cell surface receptors are pivotal in extrinsic apoptosis pathways [70-72]. Upon interaction between cell surface tumor necrosis factor receptor (TNFR) and its extracellular counterpart, receptors undergo trimerization, forming complexes with intracellular signaling molecules such as TNF receptor-linked death domain protein [73]. Our investigation observed a notable increase in TNF-α expression at both the genetic and protein levels under HG conditions. This elevation was mitigated by synergistic therapy with tFNAs, resulting in decreased TNF-α expression. This finding suggests the activation of the extracellular apoptotic pathway by HG. At the same time, tFNAs can counteract this activation by reducing TNF-α expression and impeding the binding of death receptors and ligands.

Extrinsic or intrinsic mechanisms can initiate Caspase-dependent apoptosis [74,75]. In the mitochondrial (intrinsic) apoptosis pathway, after mitochondrial membrane depolarization and the pores in membrane forming, cytochrome c is produced, and caspase-9 contributes to apoptosome formation, initiating Caspase-dependent cell apoptosis [76]. Our study also revealed a significant upregulation of the caspase-9 gene under HG conditions, which was inhibited by tFNAs treatment, indicating that the anti-apoptotic function of tFNAs can modulate the mitochondrial apoptosis pathway. Compared to the control group, the gene levels of *caspase-9* increased in HG group. Conversely, following incubation with tFNAs for 24 and 48 h, a significant decrease in *caspase-9* gene expression was observed by an average of 0.016- and 0.013-fold, respectively (Fig. 4i). In the extrinsic apoptosis pathway, the complex of death receptors and ligands interacts with caspase-8, inducing their auto-cleavage and activation [77]. Caspase-9, 8, 10 are initiator Caspases, ultimately leading to the cleavage and activation of Caspase-3, the principal effector Caspase responsible for the degradation of several cellular substrates, culminating in apoptosis-associated morphological changes [78]. The gene levels of *caspase-3* increased in the HG group, yet decreased by an average of 0.023- and 0.017-fold, respectively, following incubation with tFNAs for 24 and 48 h (Fig. 4j). Western blot outcomes (Figs. 4k and l) were consistent with the RT-PCR results. Cleaved-caspase3 expression decreased in tFNAs group after 24 and 48 h incubation compared to the HG group. A gray value analysis of Western blot bands revealed that cleaved-caspase3 in the tFNAs group after 24 h incubation decreased by 0.79-fold, and after 48 h incubation decreased by 0.56-fold. In the immunofluorescence experiments, a trend similar to BAX of the red fluorescence intensity was observed for cleaved caspase-3 expression, confirming the apoptotic state induced by the caspase-dependent apoptotic pathway (Figs. 4m and n).

In summary, the inhibition of cell apoptosis by tFNAs under HG conditions is significant and multifaceted, suggesting promis-

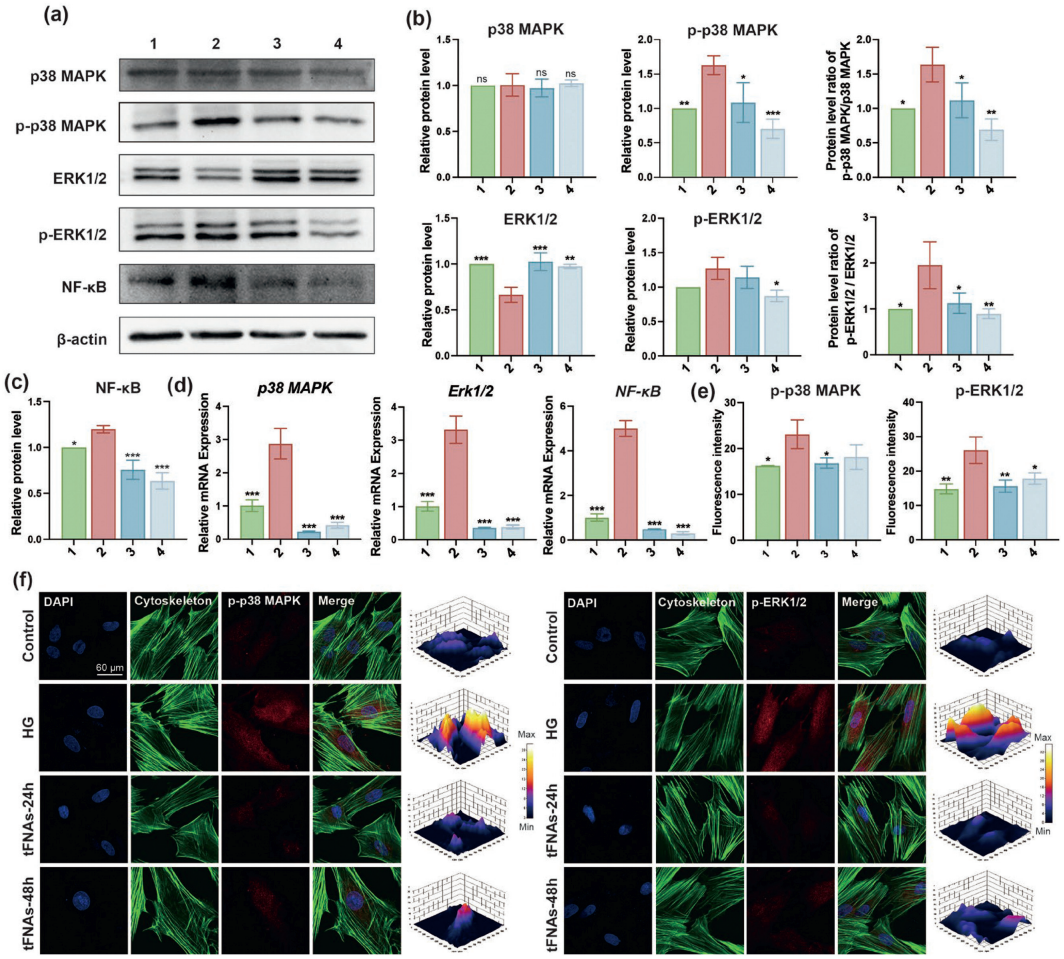

Fig. 5. tFNAs inhibit MAPK/NF-κB signaling pathway under high glucose conditions. (a–c) Western blot with statistical analysis detects pathway-related protein expression levels. (d) The relative mRNA expression intensity of pathway-related genes. (e, f) Immunofluorescence detection with statistical analysis of phosphorylated MAPK pathway proteins. Scale bar: 60 μm. Group settings: 1-control, 2-HG, 3-HG + tFNAs (24 h), 4-HG + tFNAs (48 h). Data are presented as mean ± SD ($n = 3$). $^{*}P < 0.05$, $^{**}P < 0.01$, $^{***}P < 0.001$ *vs.* HG.

ing prospects for their application in cell therapy to enhance bone repair in DM patients.

Based on prior research, the ROS/MAPK/NF-κB pathway has been implicated in the HG-induced release of inflammatory mediators [3,79,80]. The release of inflammatory factors can also originate from the direct activation of classical inflammatory pathways induced by HG, specifically the MAPK and NF-κB pathways which can be further activated through a positive feedback mechanism involving newly released inflammatory factors [81,82]. In summary, the intracellular signaling pathways and cellular responses under HG induction are intricate and ultimately lead to changes in the extracellular environment, leading to cell apoptosis in both intrinsic and external pathways [83-85]. Meanwhile, emerging data demonstrates the capacity of tFNAs to mitigate intracellular ROS production [49], inhibit MAPK phosphorylation [33], and suppress NF-κB signaling activation [60]. Thus, we delve deeper into the underlying mechanism governing DFSCs' dysfunction in HG conditions and the protective effort tFNAs make to inhibit the activation of the ROS/MAPK/NF-κB pathway.

Western blot results elucidate the inhibitory effect of tFNAs on activating the MAPKs/NF-κB pathway. Notably, p-p38, phospho-extracellular regulated kinase 1/2 (p-ERK1/2), and NF-κB protein expression escalated following HG treatment, indicating pathway activation. However, subsequent incubation with tFNAs for 24 and 48 h led to a significant decrease in these protein expressions (Fig. 5a). Specifically, statistical analysis of the Western blot data revealed a notable reduction in the ratios of p-p38/p38 and p-ERK1/2/ERK1/2 after tFNAs treatment, respectively, by 0.68- and 0.57-fold after 24 h incubation, and by 0.42- and 0.45-fold after 48 h incubation, indicative of suppressed MAPK pathway phosphorylation (Fig. 5b). Moreover, NF-κB expression decreased by 0.63- and 0.53-fold after 24 and 48 h of tFNAs treatment, respectively (Fig. 5c). To further corroborate the inhibitory effect of tFNAs on the MAPK/NF-κB pathway, gene expression levels of *p38 MAPK*, *ERK1/2*, and *NF-κB* were assessed *via* RT-PCR (Fig. 5d). Consistent with the Western blot findings, HG significantly upregulated the expression of these pathway-related genes, while subsequent tFNAs incubation for 24 and 48 h markedly attenuated their expression. Immunofluorescence analysis further supported these observations, revealing the HG group's strongest red fluorescence intensity indicative of p-p38 and p-ERK1/2 expression. Conversely, the fluorescence intensity in the tFNAs and control groups was notably weaker, underscoring the phosphorylation status of the MAPK pathways under HG conditions and following tFNAs treatment. Intuitively, the statistical analysis of immunofluorescence data among different groups of target proteins further highlighted the phosphorylation dynamics of the MAPK pathways in response to HG conditions and subsequent tFNAs treatment (Figs. 5e and f).

The ROS/MAPKs/NF-κB pathway, recognized for its ubiquitous presence and fundamental role in inflammation and cellular dysfunction, has emerged as a prime target for mitigating diabetes-related complications [3,60,86]. Our previous study has underscored tFNAs' efficacy in scavenging ROS. Herein, we substantiate these findings by proving tFNAs' capacity to inhibit MAPKs phosphorylation and suppress NF-κB pathway activation. Consistent with previous experimental outcomes, HG-treated DFSCs exhibited robust MAPKs protein phosphorylation and NF-κB protein upregulation, as confirmed by RT-PCR analyses that significant upregulation of MAPKs and NF-κB-related genes. However, upon tFNAs intervention, both 24 and 48 h treatments demonstrated significant and sustained inhibition of the MAPKs/NF-κB pathway. This inhibition is correlated with enhanced osteogenic differentiation and a substantial reduction in the apoptotic behavior of cells following treatment with tFNAs. Thus, our findings suggest that tFNAs, through modulation of the ROS/MAPKs/NF-κB pathway, create a conducive environment for DFSCs' therapeutic potential in diabetic patients, bolstering cellular functionality and therapeutic efficacy.

In summary, we proposed a nanoparticle that inhibits the ROS/MAPKs/NF-κB signaling pathway to protect DFSCs from apoptosis and restore their osteogenic differentiation ability in a high glucose model. This is vital to improving stem cell therapy in bone repair for DM patients due to the unique antioxidant and anti-inflammatory properties of tFNAs and their induction of osteogenic differentiation in MSCs. Our experiment preliminarily validated the enhancement of DFSCs treatment in DM bone repair by tFNAs, providing maximum compensation for the defects mentioned above. Moreover, our preliminary exploration of tFNAs-enhanced DFSCs therapy has opened up a new field for further development of functionalized drug-loaded tFNAs platforms to assist in stem cell therapy. The advancements stemming from our study promise to accelerate progress in combating human diabetes.

Declaration of competing interest

The authors declare that they have no known competing financial interests or personal relationships that could have appeared to influence the work reported in this paper.

CRediT authorship contribution statement

Ruijianghan Shi: Writing – review & editing, Writing – original draft, Visualization, Methodology, Investigation, Formal analysis, Data curation, Conceptualization. **Yujie Zhu:** Writing – review & editing, Methodology. **Weitong Lu:** Writing – review & editing, Methodology. **Yuhan Shao:** Writing – review & editing. **Yang Chen:** Writing – review & editing, Methodology. **Mi Zhou:** Writing – review & editing, Methodology. **Yunfeng Lin:** Writing – review & editing, Supervision, Project administration, Conceptualization. **Sirong Shi:** Writing – review & editing, Supervision, Resources, Project administration, Methodology, Funding acquisition, Conceptualization.

Acknowledgments

This study was supported by the National Natural Science Foundation of China (Nos. 82101077, 82370929), Sichuan Science and Technology Program (Nos. 2023NSFSC1516, 2023NSFSC1706), Postdoctoral Science Foundation of China (Nos. 2021M692271, 2023T160455, BX20220220, 2022M722251), West China School/Hospital of Stomatology Sichuan University (No. RCDWJS2023–5), Fundamental Research Funds for the Central Universities, and Research and Develop Program, West China Hospital of Stomatology Sichuan University. The authors would like to thank Liying Hao (State Key Laboratory of Oral Diseases, National Clinical Research Center for Oral Diseases, West China Hospital of Stomatology, Sichuan University) for her help in characterizing AFM.

Supplementary materials

Supplementary material associated with this article can be found, in the online version, at doi:10.1016/j.cclet.2024.110241.

References

[1] A. Scott, D. Chambers, E. Goyder, et al., PLoS One 12 (2017) e0177210.
[2] X. Yang, M. Bao, Y. Fang, et al., J. Transl. Med. 19 (2021) 283.
[3] Y. An, H. Zhang, C. Wang, et al., FASEB J. 33 (2019) 12515–12527.
[4] L.C. Hofbauer, B. Busse, R. Eastell, et al., Lancet Diabetes Endocrinol. 10 (2022) 207–220.
[5] L. Bai, M. Feng, Q. Zhang, et al., Adv. Funct. Mater. 12 (2024) 14.
[6] S.C. Tao, X.R. Li, W.J. Wei, et al., Biomaterials 34 (2024) 2314789.
[7] L. Yang, Y. Liu, L. Sun, et al., Nano-Micro Lett. 14 (2021) 4.

[8] R. Bi, P. Lyu, Y. Song, et al., Biomolecules 11 (2021) 997.
[9] M. Rezai-Rad, J.F. Bova, M. Orooji, et al., Cytotherapy 17 (2015) 1572–1581.
[10] X. Luan, Y. Ito, S. Dangaria, T.G. Diekwisch, Stem Cells Dev. 15 (2006) 595–608.
[11] T. Zhou, J. Pan, P. Wu, et al., Stem Cells Int. 2019 (2019) 9159605.
[12] B.W. Park, S.J. Jang, J.H. Byun, et al., J. Tissue Eng. Regen. Med. 11 (2017) 489–500.
[13] H.J. Lee, C.W. Chae, H.J. Han, Biomed. Pharmacother. 168 (2023) 115759.
[14] Q. Zhang, X.X. Wan, X.M. Hu, et al., Front. Cell. Dev. Biol. 9 (2021) 809656.
[15] L. Zhang, Z. Bei, T. Li, Z. Qian, Bioact. Mater. 29 (2023) 132–150.
[16] Y.L. Zhang, Y. An, L.J. Sun, et al., Front. Endocrinol. 14 (2023) 1152845.
[17] B. Yang, T.S. Johnson, G.L. Thomas, et al., Kidney Int. 62 (2002) 1301–1313.
[18] S. Cheng, H.N. Wang, L.J. Xu, et al., J. Neuroinflamm. 18 (2021) 182.
[19] Y. Chen, X. Chen, B. Zhang, et al., Signal Transduct. Target. Ther. 9 (2024) 28.
[20] Q. Wang, J. Cheng, F. Liu, et al., Adv. Sci. 11 (2024) 2306622.
[21] D. Xiao, T. Chen, Zhang T, et al., Chin. Chem. Lett. 35 (2024) 108602.
[22] Y. Wen, M. Zhang, Y. Yao, et al., Chin. Chem. Lett. 34 (2023) 107549.
[23] Y. Li, Z. Cai, W. Ma, et al., Bone Res. 12 (2024) 14.
[24] Y. Ge, Q. Wang, Y. Yao, et al., Adv. Sci. 11 (2024) 2308701.
[25] Y. Liu, C. Zeng, Z. Huang, et al., Chem. Eng. J. 486 (2024) 150419.
[26] J. Sun, Y. Gao, Y. Yao, et al., Chem. Eng. J. 487 (2024) 150706.
[27] W. Zou, J. Lu, L. Zhang, et al., J. Nanobiotechnol. 22 (2024) 113.
[28] S. Lin, Q. Zhang, S. Li, et al., ACS Appl. Mater. Interfaces 12 (2020) 11397–11408.
[29] M. Liu, W. Ma, Q. Li, et al., Cell Prolif. 52 (2019) e12511.
[30] Z. Wang, H. Lu, T. Tang, et al., Cell Prolif. 55 (2022) e13316.
[31] M. Zhou, N.X. Liu, S.R. Shi, et al., Nanomedicine 14 (2018) 1227–1236.
[32] B. Guo, T. Chen, D. Xiao, et al., Chin. Chem. Lett. 33 (2022) 2517–2521.
[33] M. Zhou, S. Gao, X. Zhang, et al., Bioact. Mater. 6 (2021) 1676–1688.
[34] P. Li, L. Fu, C. Ning, et al., Cell Prolif. 57 (2024) e13605.
[35] X. Chen, J. He, Y. Xie, et al., Cell Prolif. 56 (2023) e13424.
[36] W. Ma, X. Shao, D. Zhao, et al., ACS Appl. Mater. Interfaces 10 (2018) 7892–7900.
[37] D. Genç, M. Sezer Kürkçü, G. Yiğittürk, et al., Arch. Rheumatol. 37 (2022) 94–109.
[38] G. Mori, A. Ballini, C. Carbone, et al., Int. J. Med. Sci. 9 (2012) 480–487.
[39] T. Zhang, T. Tian, R. Zhou, et al., Nat. Protoc. 15 (2020) 2728–2757.
[40] L. Liang, J. Li, Q. Li, et al., Angew. Chem. Int. Ed. 53 (2014) 7745–7750.
[41] T. Tian, C. Zhang, J. Li, et al., Small 17 (2021) e2100837.
[42] J.M. Tang, J.N. Wang, L. Zhang, et al., Cardiovasc. Res. 91 (2011) 402–411.
[43] Y. Chen, T. Wu, S. Huang, et al., ACS Appl. Mater. Interfaces 11 (2019) 14608–14618.
[44] Z. Qian, H. Wang, Y. Bai, et al., ACS Appl. Mater. Interfaces 12 (2020) 55659–55674.
[45] P. Ramos-García, J.A. Gil-Montoya, C. Scully, et al., Oral Dis. 23 (2017) 897–912.
[46] W. Ren, M. Chai, M. Jiang, et al., Mol. Biol. Rep. 49 (2022) 2723–2733.
[47] T. Kawane, X. Qin, Q. Jiang, et al., Sci. Rep. 8 (2018) 13551.
[48] E. Zherebitskaya, E. Akude, D.R. Smith, P. Fernyhough, Diabetes 58 (2009) 1356–1364.
[49] Y. Yao, X. Lei, Y. Wang, et al., ACS Nano 17 (2023) 22334–22354.
[50] X. Qin, N. Li, M. Zhang, et al., Nanoscale 11 (2019) 20667–20675.
[51] H. Wei, K. Yi, F. Li, et al., Adv. Mater. 36 (2024) 2305826.
[52] H. Kim, Y.D. Lee, H.J. Kim, et al., J. Bone Miner. Res. 32 (2017) 397–406.
[53] C. Bi, Y. Ma, Z. Wu, et al., Plant. Mol. Biol. 94 (2017) 197–213.
[54] T. Wu, X. Chen, Y. Wang, et al., Nanomedicine 14 (2018) 2215–2226.
[55] M. Xiong, Y. Zhao, H. Mo, et al., Int. Immunopharmacol. 100 (2021) 108165.
[56] Y. Xu, J. Chen, W. Jiang, et al., Small 18 (2022) e2102848.
[57] X. Yin, X. Zhuang, W. Luo, et al., Front. Immunol. 13 (2022) 990297.
[58] Y. Zhang, S. Xu, K. Li, et al., Ecotoxicol. Environ. Saf. 252 (2023) 114607.
[59] H.S. Choi, A.P. Mathew, S. Uthaman, et al., J. Nanobiotechnology 20 (2022) 205.
[60] M. Zhou, T. Zhang, B. Zhang, et al., ACS Nano 16 (2022) 1456–1470.
[61] C.K. Chan, H. Supriady, B.H. Goh, H.A. Kadir, J. Ethnopharmacol. 168 (2015) 291–304.
[62] C. Park, H.J. Cha, M.Y. Kim, et al., Antioxidants 11 (2022) 2353.
[63] P.E. Czabotar, A.J. Garcia-Saez, Nat. Rev. Mol. Cell Biol. 24 (2023) 732–748.
[64] M. Certo, V. Del Gaizo Moore, M. Nishino, et al., Cancer Cell 9 (2006) 351–365.
[65] A. Nechushtan, C.L. Smith, I. Lamensdorf, et al., J. Cell Biol. 153 (2001) 1265–1276.
[66] H. Ze, T. Li, X. He, et al., Respir. Res. 21 (2020) 229.
[67] H.A. Park, K. Broman, E.A. Jonas, Neural Regen. Res. 16 (2021) 12–15.
[68] Y. Liu, X. Gong, J. Wang, et al., Environ. Toxicol. 37 (2022) 2058–2071.
[69] H. Rizwan, S. Kumar, G. Kumari, A. Pal, Life Sci. 312 (2023) 121208.
[70] C. Lou, C. Lin, W. Wang, et al., J. Ethnopharmacol. 316 (2023) 116744.
[71] F.F. Wang, P.Y. Zhao, X.J. He, et al., Front. Cell Infect. Microbiol. 12 (2022) 827750.
[72] N. Yan, Y. Liu, S. Liu, et al., Mol. Neurobiol. 53 (2016) 4449–4460.
[73] T. Sessler, S. Healy, A. Samali, E. Szegezdi, Pharmacol. Ther. 140 (2013) 186–199.
[74] C.H. Su, S.P. Chen, L.Y. Chen, et al., Ecotoxicol. Environ. Saf. 228 (2021) 112962.
[75] J. Kizhakkayil, F. Thayyullathil, S. Chathoth, Free Radic, et al., Biol. Med. 52 (2012) 1854–1864.
[76] K. Aral, C.A. Aral, Y. Kapila, J. Periodontol. 90 (2019) 288–294.
[77] L. Xu, Y. Zhang, X. Qu, et al., Mol. Oncol. 11 (2017) 1733–1751.
[78] R. Gong, D. Wang, G. Abbas, et al., Sci. China Life Sci. 65 (2022) 540–549.
[79] Z. Chen, H. Gao, L. Wang, et al., Chem. Biol. Interact. 316 (2020) 108921.
[80] C. Park, H.J. Cha, H. Hwangbo, et al., Antioxidants 12 (2023) 1410.
[81] E.S. Jo, N. Sp, D.Y. Kang, et al., Molecules 25 (2020) 2342.
[82] I. Rahman, P.S. Gilmour, L.A. Jimenez, W. MacNee, Mol. Cell Biochem. 234-235 (2002) 239–248.
[83] X. Sui, N. Kong, L. Ye, et al., Cancer Lett. 344 (2014) 174–179.
[84] Y. Li, C. Shang, Z. Liu, et al., Cell Commun. Signal 20 (2022) 134.
[85] Q. Qian, X. Cao, B. Wang, et al., J. Cell Physiol. 234 (2019) 5953–5963.
[86] N. Fujiwara, S. Yamashita, M. Okamoto, et al., Ecotoxicol. Environ. Saf. 260 (2023) 115089.